

The Toroidal Moments in Confined Nanomagnets and its Impact on Magnonics

F. Brevis,^{1,*} L. Körber,² R. A. Gallardo,¹ A. Kákay,³ and P. Landeros^{1,†}

¹*Departamento de Física, Universidad Técnica Federico Santa María, Avenida España 1680, Valparaíso, Chile*

²*Radboud University, Institute of Molecules and Materials, Heyendaalseweg 135, 6525 AJ Nijmegen, The Netherlands*

³*Helmholtz-Zentrum Dresden-Rossendorf, Institute of Ion Beam Physics and Materials Research, Bautzner Landstr. 400, 01328 Dresden, Germany*

(Dated: December 19, 2024)

The nonreciprocity created by dipolar coupling, electric currents, and Dzyaloshinskii-Moriya interactions is discussed in cases where the magnon propagation direction has a component parallel to the toroidal moment of the magnetization. A criterion for calculating the toroidal moments is established, addressing the issue of correct origin selection based on compensated and uncompensated magnetizations. This criterion is then applied to various nonreciprocal magnetic systems, with the calculations consistent with those reported in the literature and predicting the existence of nonreciprocity in a more general manner. These results broaden the physical significance of the toroidal moment and facilitate the identification and estimation of nonreciprocity in magnonic systems. This work also clarifies the interrelations between different definitions of the toroidal moment for confined structures, where a surface term arising from surface-bound currents connects these definitions without the need for time-averaging. Comparing these definitions of the toroidal moment applied to different magnetic textures demonstrates that they are always parallel but may differ in magnitude and sign. The discrepancy in the different definitions is deemed irrelevant since its direction, rather than its magnitude, primarily predicts the existence of magnon nonreciprocity.

Nonreciprocity, the asymmetric propagation of waves or signals, is a fundamental concept across various physical domains, including photonics, phononics, plasmonics, electronics, spintronics, and magnonics [1, 2]. It is crucial for developing devices that control the flow of energy or information in a single direction, preventing unwanted reflections and improving system efficiency [3, 4]. For example, nonreciprocal optical isolators ensure that light travels in one direction while being blocked or altered in reverse, which is vital for protecting optical systems [5]. In magnonics, nonreciprocity enables directional control of magnetic excitations known as spin waves (SWs), or magnons if we refer to them as quasiparticles, paving the way for technologies that enhance the performance and functionality of communication and data processing at the nanoscale [6–8], and even quantum computing [9].

Space-time symmetry breaking is an important condition for nonreciprocity. In magnetic materials, it can occur either from its interaction with quasiparticles, as photons interacting with magnetic crystals, or with magnons [10, 11]. This condition can be indicated by the definition of a toroidal moment ($\boldsymbol{\tau}$) [12–14], allowing to estimate the presence of nonreciprocity based on the equilibrium magnetization (\mathbf{M}) and wave vector (\mathbf{k}). Specifically, if $\boldsymbol{\tau} \cdot \mathbf{k} \neq 0$, then nonreciprocity is enabled [15]. The presence of $\boldsymbol{\tau}$ has been associated with the nonreciprocity of photons in a magnetic crystal [16, 17], and the nonreciprocity of spin waves in nanotubes with vortex state [15] and artificial chiral magnets with curling states [18]. Besides, such symmetry breakings are essential for the emergence of magnetoelectric effects, where the electric polarization (\mathbf{P}) couples with \mathbf{M} , as $\boldsymbol{\tau}$ is dual to the antisymmetric part of the magnetoelectric susceptibility

tensor [19]. Thus, the presence of $\boldsymbol{\tau} \times \mathbf{k}$ is a key concept in condensed matter physics [20–23].

In this Letter, the implications of an emergent toroidal moment in the context of magnonics [8, 24] are discussed and applied to a variety of systems, such as the current-induced SW Doppler shift in films [25, 26], magnetic textures [27, 28], magnetization-graded films [29], bilayers [30, 31], and films with interfacial and bulk Dzyaloshinskii-Moriya interaction (DMI) [32–35]. First, the toroidal moment derived by Dubovik and Tugushev [36] is revisited, using the concept of bound currents, showing that volume and surface contributions for $\boldsymbol{\tau}$ arises. The volume expression has been widely used to evaluate $\boldsymbol{\tau}$ [19, 37]. Nonetheless, the surface term has not yet been reported and may be relevant for studying nanostructures. Based on Ederer and Spaldin proposal to avoid the origin dependence of $\boldsymbol{\tau}$ for microscopic systems [38], a similar approach is applied to predict symmetry breaking and nonreciprocity in magnonic systems.

Proposed from multipole expansions of the vector potential [36], the toroidal moment can be understood by considering an electric current moving along the meridians of a ferrite toroidal core, generating a magnetic field and a circular \mathbf{M} . This texture produces a net $\boldsymbol{\tau}$ perpendicular to the toroid plane [39]. Microscopically, a toroidal moment $\boldsymbol{\tau} = (-g\mu_B/2) \sum_i \mathbf{r}_i \times \mathbf{S}_i$ can be viewed as a built-in effective vector potential \mathbf{A}_{eff} under the presence of spin-orbit interaction [40]. In photonics, the effective spin-orbit coupling creates a toroidal moment along the electric field, allowing the observation of ferrotoroidal domains with second harmonic generation in LiCoPO_4 [13, 41]. The same technique reveals the nonreciprocity of photons in a magnetoelectric antiferromagnet

CuB₂O₄ [17], which was first shown when the antiferromagnetic order vector is parallel to $\boldsymbol{\tau}$. It has also been demonstrated that the presence of $\boldsymbol{\tau}$ associated with the magnetoelectric effect modifies the dispersion of electromagnetic waves in a medium, with a term proportional to $\boldsymbol{\tau} \cdot \mathbf{k}$ [42], as well as the propagation of surface plasmons in nanowires [43]. In magnonics, a similar situation is described by Foggetti *et al.* [16], studying magnons in hexagonal LuFeO₃, showing that nonreciprocal spin-wave propagation is achieved when $\boldsymbol{\tau} \parallel \mathbf{k}$, both parallel to the crystal c -axis. From the symmetry of the lattice, the product $k_z(\mathbf{r}_i \times \mathbf{S}_i)_z$ is invariant, and the magnon energy has a linear term proportional to k_z (along the c -axis), giving rise to nonreciprocity [16]. The essential point is that there is no symmetry operation connecting a reciprocal situation when $\boldsymbol{\tau} \parallel \mathbf{k}$ [10, 44] because the symmetry operations will transform $\boldsymbol{\tau}$ and \mathbf{k} in the same manner. Then, any frequency asymmetry in wave propagation arising from symmetry breaking can be anticipated if the condition $\boldsymbol{\tau} \cdot \mathbf{k} \neq 0$ is fulfilled [15]. This suggests that magnon nonreciprocity can be assessed by $\boldsymbol{\tau}$, either if it arises from a free current [25, 45], a curling magnetization [18, 46], or from mirror symmetry broken by an interface (surface anisotropies, interlayer exchange coupling, or DMI) [35]. Such phenomena are consequences of Neumann's principle, which states that any symmetry shown by the point group of the crystal is adopted by its physical properties [11, 47, 48].

Several approaches for calculating $\boldsymbol{\tau}$ have been reported [19, 37]. The first expression is [36]

$$\boldsymbol{\tau} = \frac{1}{10} \int dV [\mathbf{r}(\mathbf{r} \cdot \mathbf{J}) - 2r^2 \mathbf{J}], \quad (1)$$

where \mathbf{J} corresponds to the current density, which may include free currents (\mathbf{J}_f), bound currents (\mathbf{J}_b), and polarization currents ($\partial \mathbf{P} / \partial t$) [50, 51]. For magnetic matter, the bound current is $\mathbf{J}_b = \nabla \times \mathbf{M}$. Then, in the absence of free and polarization currents, $\mathbf{J} = \mathbf{J}_b$ and the magnetic contribution to the emergent toroidal moment is given by $\boldsymbol{\tau} = \frac{1}{10} \int dV [\mathbf{r}(\mathbf{r} \cdot (\nabla \times \mathbf{M})) - 2r^2 \nabla \times \mathbf{M}]$. By utilizing standard vector identities [49], $\boldsymbol{\tau}$ splits into volumetric and surface contributions $\boldsymbol{\tau} = \boldsymbol{\tau}^v + \boldsymbol{\tau}^s$, where

$$\boldsymbol{\tau}^v = \frac{1}{2} \int dV (\mathbf{r} \times \mathbf{M}), \quad (2)$$

which was later obtained by a multipole expansion of the vector potential [19, 38]. Eq. (2) has been widely used for calculating $\boldsymbol{\tau}$ in magnetic structures [13, 14, 52–54]. Indeed, the microscopic version of the toroidal moment arises from Eq. (2) [38]. On the other hand,

$$\boldsymbol{\tau}^s = -\frac{1}{10} \oint_{\partial V} dS [\mathbf{r}(\mathbf{r} \cdot \mathbf{K}_b) - 2r^2 \mathbf{K}_b] \quad (3)$$

is due to surface-bound current $\mathbf{K}_b = \mathbf{M} \times \mathbf{n}$, with \mathbf{n} a unit vector normal to the local surface. Notice that $\boldsymbol{\tau}^s$, which has not been reported before, is

analogous to Eq. (1) but with a closed surface integral and opposite sign. Nonetheless, there is an alternative definition for the toroidal moment given by $\boldsymbol{\tau}' = (1/6) \int dV [\mathbf{r} \times (\mathbf{r} \times \mathbf{J})]$ [19, 37], which gives $\boldsymbol{\tau}' = (1/3)\boldsymbol{\tau}^v - (5/3)\boldsymbol{\tau}^s$, where $\boldsymbol{\tau}^v$ and $\boldsymbol{\tau}^s$ are the moments found before. The toroidal moment $\boldsymbol{\tau}$ and $\boldsymbol{\tau}'$ are equivalent when averaged over time if only free currents are considered [19]. Still, without this temporal average, there is a significant difference due to the surface term.

The toroidal moment can be used to predict the existence of dipolar symmetry breaking in the magnon spectrum [15]. However, one issue not considered in Ref. 15 is the proper choice of origin when calculating the volumetric toroidal moment. One can easily check, e.g. with Eq. (2), that shifting the coordinate origin by a vector \mathbf{R} changes the toroidal moment $\boldsymbol{\tau}^v \mapsto \boldsymbol{\tau}^v + (1/2) V \mathbf{R} \times \langle \mathbf{M} \rangle$, where V is the sample volume. Nonetheless, the choice of origin is not an issue if the sample has a zero magnetic moment, $\langle \mathbf{M} \rangle = 0$, such as the vortex texture [15]. One route to circumvent this origin dependence is found in Ref. 38 for localized spins, where \mathbf{M} is divided into a compensated part with zero magnetic moment $\mathbf{M}^{(0)} = \mathbf{M} - \langle \mathbf{M} \rangle$ and an uncompensated or fully polarized background $\mathbf{M}^{(1)} = \langle \mathbf{M} \rangle$. Following Ref. 38, the part of the toroidal moment due to $\langle \mathbf{M} \rangle$ cannot induce any frequency asymmetry for a homogeneous and centrosymmetric lattice (in the absence of intrinsic DMI). Therefore, the only part of the toroidal moment that is relevant for dipolar symmetry-breaking is [55]

$$\boldsymbol{\tau}^v = \frac{1}{2} \int dV \mathbf{r} \times (\mathbf{M} - \langle \mathbf{M} \rangle), \quad (4)$$

which is origin-independent, as it involves only the compensated magnetization. While $\boldsymbol{\tau}$ can be estimated using Eqs. (1-4), in general their different definitions are parallel to each other [49]. Then, $\boldsymbol{\tau} \cdot \mathbf{k}$ can be calculated using any of these definitions. In the following examples, the different definitions of the toroidal moment are used to analyze the nonreciprocity phenomena in different magnetic systems. Here, it is emphasized that Eq. (1) is suitable to connect the toroidal moment with nonreciprocal wave phenomena when only free currents are present ($\mathbf{J} = \mathbf{J}_f$). In the absence of free currents, and for nonuniform magnetization textures, Eqs. (3-4) are used to capture the proper relation between the wave propagation and the toroidal moment [56].

By considering a constant electric current density \mathbf{J}_f flowing through a film with volume V , one finds, from Eq. (1), $\boldsymbol{\tau} \propto -V \mathbf{J}_f$. Consequently, the nonreciprocity condition gives $\boldsymbol{\tau} \cdot \mathbf{k} \propto -\mathbf{J}_f \cdot \mathbf{k}$, which is nonzero if the wave vector includes a component along the current. Such a statement perfectly agrees with earlier works. Indeed, an electric current, via spin-transfer torque, produces a linear term in the magnonic dispersion associated with a Doppler shift $\Delta f \propto \mathbf{J}_f \cdot \mathbf{k}$, which has been predicted by theory [45, 57] and measured experimentally [25, 26]

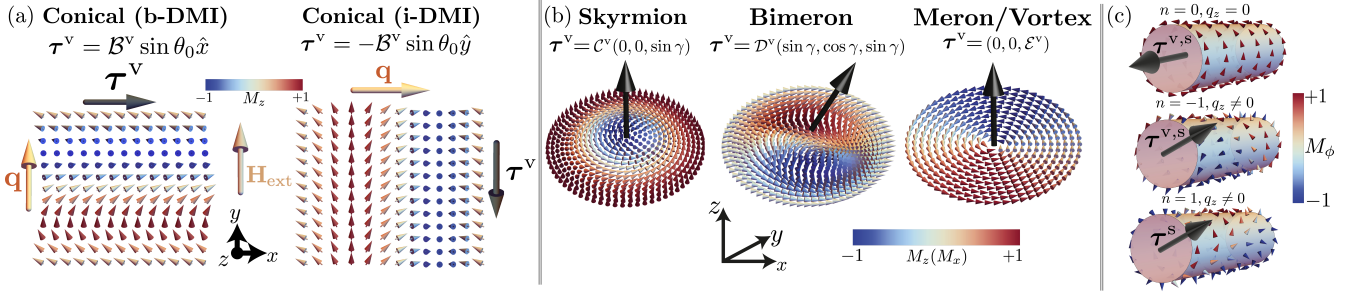


FIG. 1. (a) Volume toroidal moment for the conical-helix textures with bulk and interfacial DM, for $\psi = \pi/2$ and $\theta_0 = \pi/3$. (b) Volume toroidal moments for skyrmion, bimeron, and meron/vortex textures. Schematics show the magnetization texture for $\gamma = \pi/2$. Coloring according to the $z(x)$ -component for skyrmion and bimeron (meron). The \mathcal{C}^v , \mathcal{D}^v , and \mathcal{E}^v can be found in the supplementary material [49]. (c) Conical-helix texture on a nanotube with i-DMI. From top to bottom: State with $n = 0$ and $q_z = 0$, τ^v points along the axis. State with $n = -1$ and state with $n = 1$, both with finite q_z and $\tau^{v,s}$ is perpendicular to the axis. Coloring according to the azimuthal direction of magnetization.

for a saturated magnetic film. Therefore, a free electric current creates a toroidal moment and a nonreciprocal wave behavior, even in the case of uniform magnetization.

In the absence of free currents but in the presence of noncollinear forms of the magnetization that may exhibit helicity or chirality [58–60], a toroidal moment may emerge from a bound current. Examples are conical-helix (Bloch or Néel type) [61–65], vortex-like [15], skyrmion-like [66–68], and hopfion-like magnetic textures [69, 70]. A conical-helix (CH) texture, stabilized by a DMI, can be modeled as $\mathbf{M}(\mathbf{r}) = M_s(\sin[\mathbf{q} \cdot \mathbf{r} + \psi] \sin \theta, \cos \theta, \cos[\mathbf{q} \cdot \mathbf{r} + \psi] \sin \theta)$, where M_s is the saturation magnetization and $\mathbf{q} = q(\sin \varphi_{\mathbf{q}}, \cos \varphi_{\mathbf{q}}, 0)$ is the in-plane pitch vector that establishes the direction of the texture variation according to $\varphi_{\mathbf{q}}$ [65]. For bulk DMI (b-DMI), the angle $\varphi_{\mathbf{q}} = 0$ produces a Bloch-like texture. Instead, for interfacial DMI (i-DMI), $\varphi_{\mathbf{q}} = \pi/2$ induces a Néel-like texture. The phase angle ψ must be accounted for finite systems and is related to the tendency of \mathbf{M} to orient in-plane or out-of-plane due to the competition between the dipolar field and perpendicular anisotropy [65]. Also, θ is the cone angle related to the tilting around the external field ($\mathbf{H} = H\hat{y}$), so that $\theta = \pi/2$ describes a perfect helix, while $\theta = 0$ defines the polarized state along the field. The toroidal moment for the conical-helix, either with bulk or interfacial DMI, gives $\tau^v = \mathcal{B}^v \sin \theta(\sin \psi \cos \varphi_{\mathbf{q}}, -\sin \psi \sin \varphi_{\mathbf{q}}, \cos \psi \cos \varphi_{\mathbf{q}})$, where $\mathcal{B}^v = \frac{M_s L d}{2q^2} [Lq \cos(Lq/2) - 2 \sin(Lq/2)]$, considering a square film with volume $V = L^2 d$ and thickness d .

For this texture, τ^v is always parallel or antiparallel to τ^s [49]. Fig. 1(a) illustrates the volume toroidal moment directions for conical-helix magnetic textures. These results and the nonreciprocity condition are consistent with Ref. 27, where asymmetric dispersions were reported for SWs excited over CH states in a Cu_2OSeO_3 single crystal with bulk DMI. Here, a frequency shift was observed for spin waves with a wavevector parallel to $\tau^v = \tau_x^v \hat{x}$

(and perpendicular to \mathbf{H}) [27], which is not the case for uniformly magnetized films with bulk DMI, where nonreciprocity occurs for $\mathbf{k} \parallel \mathbf{H}$ [32]. The difference arises solely from the texture. In the case of an arbitrary periodic texture, the magnetization can be expanded using a Fourier series in terms of reciprocal vectors \mathbf{G} . Here, it is found that the toroidal moment is always perpendicular to \mathbf{G} , as shown in Fig. 1(a) for conical-helix textures with interfacial and bulk DMI when $\mathbf{G} \rightarrow \mathbf{q}$.

Skyrmionic textures in confined nanostructures also produce a τ^v pointing out of the plane for the meron/vortex, skyrmion, and bimeron, with the latter also exhibiting an in-plane component. Fig. 1(b) illustrates the volume toroidal moments based on analytical models for a disk with radius R and thickness d [49], where the helicity $\gamma = 0$ ($\pi/2$) corresponds to a Néel (Bloch) skyrmion. As an extension, it is also possible to model skyrmioniums/bimeroniums or $\ell\pi$ -skyrmions/bimerons, where $\ell = 1, 2, 3, \dots$ and $R = \ell\lambda$, with λ being the texture period along the radial direction. These magnetic textures are composed of a combination of skyrmions or multiple full spin rotations along the diameter with a different topological charge [71–74]. These toroidal moment calculations are consistent with those observed for skyrmion strings [28, 75], where the magnetization induces a toroidal moment parallel to their axis, and the nonreciprocal wave effect is produced along such an axis [28]. It is worth mentioning that for anti-skyrmions, the toroidal moments are always zero. From these results, one can expect similar behavior for SWs propagating along bimeron-like structures such as strings or lattices since its toroidal moment, depending on γ , can point in any of the three main directions.

Another exciting example is magnon propagation along the axis of nanotubes with magnetization in vortex or curling states, where asymmetric dispersions originating from the magnetostatic interaction have been predicted [15, 46, 76–79] and measured [80]. For a vortex configu-

ration, $\boldsymbol{\tau}^v$ is parallel to the tube axis [15], explaining the emergence of dipolar nonreciprocity along the axis. Interestingly, by including an interfacial DMI in an ultra-thin nanotube, conical-helix textures are expected similarly to planar films [81, 82]. However, unlike the flat films, the tubular systems feature quantized modes along the azimuthal direction, characterized by the integer n and a pitch vector along the tube axis ($\mathbf{q} = q_z \hat{z}$) [49]. The volume and surface toroidal moments associated with these textures are only nonzero for the curling state ($n = 0$) with $\boldsymbol{\tau}^{v,s} \parallel \hat{z}$ and the uniform transverse mode ($n = -1$) with finite q_z and $\boldsymbol{\tau}^{v,s} \perp \hat{z}$ as illustrated in Fig. 1(c). Nonetheless, the surface toroidal moment ($\boldsymbol{\tau}^s$) is also nonzero for the $n = 1$ state [49] something that Eq. (4) does not capture since $\boldsymbol{\tau}^v = 0$. Thus, based on the toroidal moment calculations, only the states $n = 0, \pm 1$ could exhibit frequency nonreciprocity of dipolar origin.

From Eq. (4), one can note that a constant M_s results in $\boldsymbol{\tau}^v = 0$. However, if M_s is spatially dependent, a nonzero $\boldsymbol{\tau}^v$ can arise even if a field polarizes the magnetization. Consider $\mathbf{M} = M_s(\mathbf{r})\mathbf{m}$, with $\mathbf{m} = (m_x, m_y, m_z)$ being the unitary magnetization. If the gradation of M_s along an arbitrary direction (\mathbf{g}), i.e., $M_s(\mathbf{r}) = M_s(x_g)$, where x_g represents the gradation coordinate, then the average magnetization is $\langle \mathbf{M} \rangle = (1/L_g) \int dx_g M_s(x_g) \mathbf{m} \equiv \langle M_s \rangle \mathbf{m}$. Therefore, the toroidal moment of the graduated system is

$$\boldsymbol{\tau}^v = \frac{V}{2L_g} \mathbf{g} \times \mathbf{m} \int_{-L_g/2}^{L_g/2} x_g [M_s(x_g) - \langle M_s \rangle] dx_g. \quad (5)$$

Clearly if $M_s(x_g)$ is constant then the integral vanishes and $\boldsymbol{\tau}^v = 0$. For a linear gradation profile $M_s(x_g) = \langle M_s \rangle + \frac{\Delta M_s}{L_g} x_g$, where ΔM_s represents the total variation of the saturation magnetization from one extreme to the other, the resulting toroidal moment reads

$$\boldsymbol{\tau}^v = \frac{VL_g}{24} \Delta M_s (\mathbf{g} \times \mathbf{m}). \quad (6)$$

An example of a graduated system is depicted in Fig. 2(a). Based on this, it follows that if $(\mathbf{g} \times \mathbf{m}) \parallel \mathbf{k}$, then SW nonreciprocity would occur as predicted [29]. In contrast, the system should be reciprocal if $(\mathbf{g} \times \mathbf{m}) \perp \mathbf{k}$, as reported in [83]. Note that the integral vanishes for any symmetric profile centered at $x_g = 0$. A specific class of magnetization-graded systems can be achieved using two ferromagnetic layers made of different materials in direct contact, each one uniformly magnetized. Here, $M_s(x_g)$ changes abruptly, and the bilayer can then be regarded as a graded system with a sharp step in M_s at the interface. Nonreciprocal waves have been measured with Brillouin light scattering in parallelly magnetized Ni/NiFe [84], and CoFeB/NiFe bilayers [85], in perfect agreement with the predictions of Eq. (6).

In the specific case of a bilayer composed of two films with top/bottom surface area L^2 , different thick-

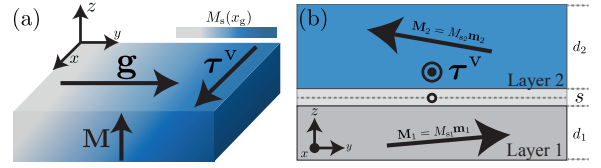


FIG. 2. (a) Ferromagnetic film with $\mathbf{M} = M_s(x_g)\hat{z}$, where there is a graded saturation magnetization along a specific direction (\mathbf{g}). This graded system exhibits a toroidal moment oriented perpendicular to \mathbf{M} and \mathbf{g} , depending on the gradient profile. (b) Asymmetric ferromagnetic bilayer. The layers have a thickness $d_{1,2}$ and magnetizations $\mathbf{M}_{1,2} = M_{s1,2}\mathbf{m}_{1,2}$. The toroidal moment is measured from the center of the spacer of thickness s . For such a configuration, the toroidal moment points in the x -direction.

nesses ($d_{1,2}$) and saturation magnetizations ($M_{s1,2}$), separated by a nonmagnetic spacer of thickness s , as seen in Fig. 2(b). Depending on whether the magnetization in the lower layer $\mathbf{M}_1 = M_{s1}\mathbf{m}$ and upper layer $\mathbf{M}_2 = \sigma M_{s2}\mathbf{m}$ are parallel ($\sigma = +1$) or antiparallel ($\sigma = -1$), the average magnetization field is

$$\langle \mathbf{M} \rangle = \frac{M_{s1}d_1 + \sigma M_{s2}d_2}{d_1 + d_2} \mathbf{m} \equiv \langle M \rangle \mathbf{m}, \quad (7)$$

and the toroidal moment, according to Eq. (5), becomes

$$\boldsymbol{\tau}^v = -\frac{L^2 d_1 d_2 (d_1 + d_2 + 2s)}{4 (d_1 + d_2)} (M_{s1} - \sigma M_{s2}) (\hat{z} \times \mathbf{m}). \quad (8)$$

This expression explicitly shows that the toroidal moment vanishes only for bilayers with parallel magnetizations ($\sigma = 1$) and $M_{s1} = M_{s2}$. In all other cases, where the bilayers have antiparallel magnetizations, or they are parallel but with different M_s , the toroidal moment suggests that nonreciprocity occurs for SWs propagating parallel to $\hat{z} \times \mathbf{m}$, with z being normal to the film's surface, as has been already reported [30]. Nonetheless, these calculations also predict nonreciprocity in much more complex systems, such as multilayers of magnetic materials with different geometries. Through simple calculations, it can be shown, for instance, that an antiferromagnetically coupled multilayer system (with magnetizations oriented along $\pm y$), with identical M_s and thicknesses, exhibits a nonzero toroidal moment along the in-plane x -direction if the number of layers is even. In contrast, when the number of layers is odd, the toroidal moment is zero. Therefore, nonreciprocity is expected in the former case but not in the latter.

Interestingly, the work of Kuznetsov and Fraerman [86] theoretically investigated spin-wave nonreciprocity in hybrid films consisting of a thin ferromagnet (FM) coupled with either a paramagnet (PM) or a superconductor (SC) semi-infinite layer. In both cases, the nonreciprocity originates from the dipolar interaction between the FM layer and the PM/SC material, which breaks the symmetry along the normal direction. In the FM/PM case, the spin

waves induce a dynamic magnetization in the paramagnet, which in turn creates an asymmetric dipolar field that influences the SW propagation. Then, the FM/PM bilayer behaves as the graded system presented earlier, where the induced dynamic magnetization in the paramagnet results in a symmetry breaking associated with a toroidal moment perpendicular to the equilibrium magnetization and the interface normal, in agreement with Eq. (6). For the FM/SC system, SWs in the FM induce a superconducting current in the SC, which also creates an asymmetric dipole field that breaks the symmetry. This inhomogeneous field within the ferromagnet can be associated with a toroidal moment parallel to $\mathbf{n} \times \mathbf{m}$ [87].

Dzyaloshinskii-Moriya materials may also present a toroidal moment [88]. For interfacial DMI, nonreciprocity is present for $\mathbf{M} \perp \mathbf{k}$, meanwhile for bulk DMI, nonreciprocity appears for $\mathbf{M} \parallel \mathbf{k}$ [32–34]. From microscopic calculations, modulations in the dispersion bands can be expressed through magnetic toroidal bond multipoles linked to anisotropic current distributions in some systems [89, 90]. These expressions are useful for predicting or estimating nonreciprocity and transport properties. From such multipole description for microscopic systems, it is also possible to obtain a toroidal moment associated with the type of DMI, the crystal lattice, and the magnetic configuration [35]. This quantity, referred to as bond magnetic toroidal dipole (BMTD), is a microscopic indicator of DMI-induced nonreciprocity and fulfills the condition $\boldsymbol{\tau} \cdot \mathbf{k} \neq 0$ for asymmetric dispersions. The BMTD is calculated using $\boldsymbol{\tau}^{(ij)} \cdot \hat{\mathbf{r}}^{(ij)} = \mathbf{D}^{(ij)} \cdot \mathbf{M}^{(ij)}$, where $\mathbf{M}^{(ij)}$ is the averaged magnetic moment for the i th and j th spins, $\hat{\mathbf{r}}^{(ij)}$ is the unit vector connecting these spins, and $\boldsymbol{\tau}^{(ij)}$ represents the bond magnetic toroidal dipole on the bond (ij) [35]. Therefore, the BMTD is active if $\mathbf{D}^{(ij)} \cdot \mathbf{M}^{(ij)} \neq 0$ and then, nonreciprocity due to DMI arises for magnons moving parallel to BMTD. For interfacial DMI, it is known that the DM vector ($\mathbf{D}^{(ij)}$) is perpendicular to $\hat{\mathbf{r}}^{(ij)}$ and nonreciprocity appears for $\mathbf{M} \perp \mathbf{k}$, meanwhile for bulk DMI the DM vector is parallel to $\hat{\mathbf{r}}^{(ij)}$, and nonreciprocity can occur for $\mathbf{M} \parallel \mathbf{k}$, in perfect agreement with well-known results [32–34]. These two situations are illustrated in Fig. 3, where two square lattices are schematized at whose sites there are localized spins in the presence of DMI. These magnetic moments are aligned along the x -axis due to a bias field so that the average magnetization in each bond points in that direction. In Fig. 3(a), interfacial DMI is considered, while in Fig. 3(b), bulk DMI is depicted. Thus, in (a) [(b)] the DM vector points perpendicular [parallel] to the vector joining two consecutive sites ($\hat{\mathbf{r}}^{(i,j)}$), representing the condition for an active BMTD to occur on each bond.

To conclude, the relationship between different definitions of the toroidal moment applied to confined magnetic structures has been elucidated, where a surface toroidal moment arising from surface-bound currents connects them without the need for time-averaging. By

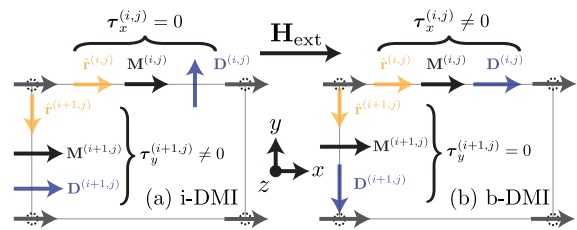


FIG. 3. BMTD for a square crystal lattice with magnetization and applied field parallel to the x -axis for a configuration with (a) i-DMI and (b) b-DMI. At the corners is the magnetization of each site (all oriented in the x -direction) and on the bonds is the unit vector that connect them, the average magnetization and the DM vector, with these three elements we obtain the BMTD associated with each configuration.

comparing these quantities applied to well-known magnetic textures, it is found that they are always parallel and may differ in magnitude and sign. For this reason, the surface toroidal moment can be very useful from the experimental point of view for samples with homogeneous textures: it is enough to know the surface magnetization to estimate its toroidal moment. Since one of the main motivations in this work relates to the prediction of magnon nonreciprocity, which is primarily determined by the toroidal moment direction and not by its magnitude, the discrepancy in the magnitude of the quantities is irrelevant. The dipolar nonreciprocity is discussed when the propagation direction of spin waves has a component parallel to the toroidal moment. Furthermore, a criterion is established for calculating it, avoiding the issue of correct origin selection based on compensated and uncompensated systems. Finally, this criterion is applied to various nonreciprocal systems, where the calculations are consistent with those reported in the literature and predict the existence of nonreciprocity in a more general way. Additionally, a toroidal moment for systems with DMI is discussed, demonstrating nonreciprocity under given conditions. These results could expand the discussion of the toroidal moment and facilitate the identification and estimation of nonreciprocity in magnonic systems mediated by dipolar and antisymmetric exchange interactions.

Acknowledgments— F.B. acknowledges support from ANID PhD grant 2021-21211469 and from USM through PIIC program. Financial support from Fondecyt grants 1241589 and 1210607, and Basal Program for Centers of Excellence, Grant AFB220001 (CEDENNA), is kindly acknowledged. L.K. gratefully acknowledges funding by the Radboud Excellence Initiative.

* felipe.brevis@usm.cl

† pedro.landeros@usm.cl

[1] R. Camley, Nonreciprocal surface waves, *Surf. Sci. Rep*

- 7**, 103 (1987).
- [2] C. Caloz, A. Alù, S. Tretyakov, D. Sounas, K. Achouri, and Z.-L. Deck-Léger, Electromagnetic nonreciprocity, *Phys. Rev. Appl.* **10**, 047001 (2018).
 - [3] T. Kodera, D. L. Sounas, and C. Caloz, Magnetless non-reciprocal metamaterial (mnm) technology: Application to microwave components, *IEEE Trans. Microw. Theory Tech.* **61**, 1030 (2013).
 - [4] C. W. Peterson, S. Kim, J. T. Bernhard, and G. Bahl, Synthetic phonons enable nonreciprocal coupling to arbitrary resonator networks, *Sci. Adv.* **4**, eaat0232 (2018).
 - [5] Y. Shi, Z. Yu, and S. Fan, Limitations of nonlinear optical isolators due to dynamic reciprocity, *Nat. Photon.* **9**, 388 (2015).
 - [6] T. An, V. I. Vasyuchka, K. Uchida, A. V. Chumak, K. Yamaguchi, K. Harii, J. Ohe, M. B. Jungfleisch, Y. Kajiwara, H. Adachi, B. Hillebrands, S. Maekawa, and E. Saitoh, Unidirectional spin-wave heat conveyer, *Nat. Mater.* **12**, 549 (2013).
 - [7] J. Chen, H. Yu, and G. Gubbiotti, Unidirectional spin-wave propagation and devices, *J. Phys. D: Appl. Phys.* **55**, 123001 (2021).
 - [8] B. Flebus, D. Grundler, B. Rana, Y. Otani, I. Barsukov, A. Barman, G. Gubbiotti, P. Landeros, J. Akerman, U. Ebels, P. Pirro, V. E. Demidov, K. Schultheiss, G. Csaba, Q. Wang, F. Ciubotaru, D. E. Nikonov, P. Che, R. Hertel, T. Ono, D. Afanasiev, J. Mentink, T. Rasing, B. Hillebrands, S. V. Kusminskiy, W. Zhang, C. R. Du, A. Finco, T. van der Sar, Y. K. Luo, Y. Shiota, J. Sklepnar, T. Yu, and J. Rao, The 2024 magnonics roadmap, *J. Phys. Condens. Matter* **36**, 363501 (2024).
 - [9] Z. Jiang, J. Lim, Y. Li, W. Pfaff, T.-H. Lo, J. Qian, A. Schleife, J.-M. Zuo, V. Novosad, and A. Hoffmann, Integrating magnons for quantum information, *Appl. Phys. Lett.* **123**, 130501 (2023).
 - [10] S.-W. Cheong, D. Talbayev, V. Kiryukhin, and A. Saxena, Broken symmetries, non-reciprocity, and multiferroicity, *npj Quantum Mater.* **3**, 19 (2018).
 - [11] D. Szaller, S. Bordács, and I. Kézsmárki, Symmetry conditions for nonreciprocal light propagation in magnetic crystals, *Phys. Rev. B* **87**, 014421 (2013).
 - [12] A. A. Gorbatsevich and Y. V. Kopaev, Toroidal order in crystals, *Ferroelectrics* **161**, 321 (1994).
 - [13] A. S. Zimmermann, D. Meier, and M. Fiebig, Ferroic nature of magnetic toroidal order, *Nat. Commun.* **5**, 4796 (2014).
 - [14] J. Lehmann, C. Donnelly, P. M. Derlet, L. J. Heyderman, and M. Fiebig, Poling of an artificial magneto-toroidal crystal, *Nat. Nanotechnol.* **14**, 141 (2018).
 - [15] L. Körber, R. Verba, J. A. Otálora, V. Kravchuk, J. Lindner, J. Fassbender, and A. Kákay, Curvilinear spin-wave dynamics beyond the thin-shell approximation: Magnetic nanotubes as a case study, *Phys. Rev. B* **106**, 014405 (2022).
 - [16] F. Foggetti, S.-W. Cheong, and S. Artyukhin, Magnetic monopoles and toroidal moments in LuFeO₃ and related compounds, *Phys. Rev. B* **100**, 180408 (2019).
 - [17] J. Mund, D. R. Yakovlev, A. N. Poddubny, R. M. Dubrovinn, M. Bayer, and R. V. Pisarev, Toroidal non-reciprocity of optical second harmonic generation, *Phys. Rev. B* **103**, L180410 (2021).
 - [18] M. Xu, A. J. M. Deenen, H. Guo, and D. Grundler, Room temperature realization of artificial chiral magnets with reprogrammable magnon nonreciprocity at zero field (2024), [arXiv:2404.19153 \[cond-mat.mtrl-sci\]](https://arxiv.org/abs/2404.19153).
 - [19] N. A. Spaldin, M. Fiebig, and M. Mostovoy, The toroidal moment in condensed-matter physics and its relation to the magnetoelectric effect, *J. Phys. Condens. Matter* **20**, 434203 (2008).
 - [20] S. Marauska, R. Jahns, H. Greve, E. Quandt, R. Knöchel, and B. Wagner, MEMS magnetic field sensor based on magnetoelectric composites, *J. Micromech. Microeng.* **22**, 065024 (2012).
 - [21] R. Policia, A. C. Lima, N. Pereira, E. Calle, M. Vázquez, S. Lanceros-Mendez, and P. Martins, Transparent magnetoelectric materials for advanced invisible electronic applications, *Adv. Electron. Mater.* **5**, 1900280 (2019).
 - [22] M. PourhosseiniAsl, X. Gao, S. Kamalishahroudi, Z. Yu, Z. Chu, J. Yang, H.-Y. Lee, and S. Dong, Versatile power and energy conversion of magnetoelectric composite materials with high efficiency via electromechanical resonance, *Nano Energy* **70**, 104506 (2020).
 - [23] X. Liang, A. Matyushov, P. Hayes, V. Schell, C. Dong, H. Chen, Y. He, A. Will-Cole, E. Quandt, P. Martins, J. McCord, M. Medarde, S. Lanceros-Mendez, S. van Dijken, N. X. Sun, and J. Sort, Roadmap on magnetoelectric materials and devices, *IEEE Trans. Magn.* **57**, 1 (2021).
 - [24] A. Barman, G. Gubbiotti, S. Ladak, A. O. Adeyeye, M. Krawczyk, J. Gräfe, C. Adelman, S. Coto-fana, A. Naeemi, V. I. Vasyuchka, B. Hillebrands, S. A. Nikitov, H. Yu, D. Grundler, A. V. Sadovnikov, A. A. Grachev, S. E. Sheshukova, J.-Y. Duquesne, M. Marangolo, G. Csaba, W. Porod, V. E. Demidov, S. Urazhdin, S. O. Demokritov, E. Albisetti, D. Petti, R. Bertacco, H. Schultheiss, V. V. Kruglyak, V. D. Poimanov, S. Sahoo, J. Sinha, H. Yang, M. Müntenberg, T. Moriyama, S. Mizukami, P. Landeros, R. A. Gallardo, G. Carlotti, J.-V. Kim, R. L. Stamps, R. E. Camley, B. Rana, Y. Otani, W. Yu, T. Yu, G. E. W. Bauer, C. Back, G. S. Uhrig, O. V. Dobrovolskiy, B. Budinska, H. Qin, S. van Dijken, A. V. Chumak, A. Khitun, D. E. Nikonov, I. A. Young, B. W. Zingsem, and M. Winklhofer, The 2021 magnonics roadmap, *J. Phys. Condens. Matter* **33**, 413001 (2021).
 - [25] V. Vlaminck and M. Bailleul, Current-induced spin-wave doppler shift, *Science* **322**, 410–413 (2008).
 - [26] M. Zhu, C. L. Dennis, and R. D. McMichael, Temperature dependence of magnetization drift velocity and current polarization in ni₈₀fe₂₀ by spin-wave doppler measurements, *Phys. Rev. B* **81**, 140407 (2010).
 - [27] N. Ogawa, L. Köhler, M. Garst, S. Toyoda, S. Seki, and Y. Tokura, Nonreciprocity of spin waves in the conical helix state, *PNAS* **118**, e2022927118 (2021).
 - [28] S. Seki, M. Garst, J. Waizner, R. Takagi, N. D. Khanh, Y. Okamura, K. Kondou, F. Kagawa, Y. Otani, and Y. Tokura, Propagation dynamics of spin excitations along skyrmion strings, *Nat. Commun.* **11**, 256 (2020).
 - [29] R. A. Gallardo, P. Alvarado-Seguel, T. Schneider, C. Gonzalez-Fuentes, A. Roldán-Molina, K. Lenz, J. Lindner, and P. Landeros, Spin-wave non-reciprocity in magnetization-graded ferromagnetic films, *New J. Phys.* **21**, 033026 (2019).
 - [30] R. Gallardo, T. Schneider, A. Chaurasiya, A. Oelschlägel, S. Arekapudi, A. Roldán-Molina, R. Hübner, K. Lenz, A. Barman, J. Fassbender, J. Lindner, O. Hellwig, and P. Landeros, Reconfigurable spin-wave nonreciprocity induced by dipolar interaction in a coupled ferromagnetic

- bilayer, *Phys. Rev. Appl.* **12**, 034012 (2019).
- [31] E. Albisetti, S. Tacchi, R. Silvani, G. Scaramuzzi, S. Finizio, S. Wintz, C. Rinaldi, M. Cantoni, J. Raabe, G. Carlotti, R. Bertacco, E. Riedo, and D. Petti, Optically inspired nanomagnonics with nonreciprocal spin waves in synthetic antiferromagnets, *Adv. Mater.* **32**, 1906439 (2020).
- [32] D. Cortés-Ortuño and P. Landeros, Influence of the dzyaloshinskii-moriya interaction on the spin-wave spectra of thin films, *J. Phys. Condens. Matter* **25**, 156001 (2013).
- [33] R. A. Gallardo, D. Cortés-Ortuño, R. E. Troncoso, and P. Landeros, Spin waves in thin films and magnonic crystals with Dzyaloshinskii-Moriya interactions, in *Three-Dimensional Magnonics*, edited by G. Gubbiotti (Jenny Stanford Publishing, Berlin, Heidelberg, 2019) pp. 121–160.
- [34] M. Kuepferling, A. Casiraghi, G. Soares, G. Durin, F. Garcia-Sanchez, L. Chen, C. H. Back, C. H. Marrows, S. Tacchi, and G. Carlotti, Measuring interfacial Dzyaloshinskii-Moriya interaction in ultrathin magnetic films, *Rev. Mod. Phys.* **95**, 015003 (2023).
- [35] T. Matsumoto and S. Hayami, Nonreciprocal magnon excitations by the dzyaloshinskii-moriya interaction on the basis of bond magnetic toroidal multipoles, *Phys. Rev. B* **104**, 134420 (2021).
- [36] V. Dubovik and V. Tugushev, Toroid moments in electrodynamics and solid-state physics, *Phys. Rep.* **187**, 145 (1990).
- [37] N. Talebi, S. Guo, and P. A. van Aken, Theory and applications of toroidal moments in electrodynamics: their emergence, characteristics, and technological relevance, *Nanophotonics* **7**, 93 (2017).
- [38] C. Ederer and N. A. Spaldin, Towards a microscopic theory of toroidal moments in bulk periodic crystals, *Phys. Rev. B* **76**, 214404 (2007).
- [39] N. Papasimakis, V. A. Fedotov, V. Savinov, T. A. Raybould, and N. I. Zheludev, Electromagnetic toroidal excitations in matter and free space, *Nat. Mater.* **15**, 263 (2016).
- [40] Y. Tokura and N. Nagaosa, Nonreciprocal responses from non-centrosymmetric quantum materials, *Nat. Commun.* **9**, 3740 (2018).
- [41] B. B. Van Aken, J.-P. Rivera, H. Schmid, and M. Fiebig, Observation of ferrotoroidic domains, *Nature* **449**, 702 (2007).
- [42] A. N. Kalish and A. K. Zvezdin, Optical properties of toroidal media, in *ICONO 2007: Novel Photonics Materials; Optics and Optical Diagnostics*, edited by O. A. Aktsipetrov, V. M. Shalaev, S. V. Gaponenko, and N. I. Zheludev, International Society for Optics and Photonics (SPIE, 2007) p. 67283D.
- [43] N. A. Gusev, V. I. Belotelov, and A. K. Zvezdin, Surface plasmons in nanowires with toroidal magnetic structure, *Opt. Lett.* **39**, 4108 (2014).
- [44] X. Xu, F.-T. Huang, and S.-W. Cheong, Magnetic toroidicity, *J. Phys. Condens. Matter* **36**, 203002 (2024).
- [45] J. Fernández-Rossier, M. Braun, A. S. Núñez, and A. H. MacDonald, Influence of a uniform current on collective magnetization dynamics in a ferromagnetic metal, *Phys. Rev. B* **69**, 174412 (2004).
- [46] R. A. Gallardo, P. Alvarado-Seguel, and P. Landeros, High spin-wave asymmetry and emergence of radial standing modes in thick ferromagnetic nanotubes, *Phys. Rev. B* **105**, 104435 (2022).
- [47] R. Birss, *Symmetry and Magnetism*, Selected topics in solid state physics (North-Holland Publishing Company, 1964).
- [48] L. D. Landau, J. S. Bell, M. Kearsley, L. Pitaevskii, E. Lifshitz, and J. Sykes, *Electrodynamics of continuous media*, Vol. 8 (Elsevier, 2013).
- [49] [URL will be inserted by publisher.](#)
- [50] J. D. Jackson, *Classical electrodynamics*, 3rd ed. (Wiley, New York, NY, 1999).
- [51] D. J. Griffiths, *Introduction to Electrodynamics*, 4th ed. (Cambridge University Press, 2017).
- [52] L. Ding, X. Xu, H. O. Jeschke, X. Bai, E. Feng, A. S. Alemany, J. Kim, F.-T. Huang, Q. Zhang, X. Ding, N. Harrison, V. Zapf, D. Khomskii, I. I. Mazin, S.-W. Cheong, and H. Cao, Field-tunable toroidal moment in a chiral-lattice magnet, *Nat. Commun.* **12**, 5339 (2021).
- [53] F. Thöle, A. Keliri, and N. A. Spaldin, Concepts from the linear magnetoelectric effect that might be useful for antiferromagnetic spintronics, *J. Appl. Phys.* **127**, 213905 (2020).
- [54] S.-W. Cheong and X. Xu, Magnetic chirality, *npj Quantum Mater.* **7**, 40 (2022).
- [55] From this point forward, τ^v will refer to Eq. (4), a more general formulation compared to Eq. (2).
- [56] In the following, the symbol τ will be used to denote any kind of toroidal moment unless it is necessary to specify a volume or a surface toroidal moment.
- [57] P. Lederer and D. L. Mills, Possible experimental test of the band theory of magnetism, *Phys. Rev.* **148**, 542 (1966).
- [58] X. Yu, M. Mostovoy, Y. Tokunaga, W. Zhang, K. Kimoto, Y. Matsui, Y. Kaneko, N. Nagaosa, and Y. Tokura, Magnetic stripes and skyrmions with helicity reversals, *PNAS* **109**, 8856 (2012).
- [59] H. Yu, J. Xiao, and H. Schultheiss, Magnetic texture based magnonics, *Phys. Rep.* **905**, 1 (2021).
- [60] T. Yu, Z. Luo, and G. E. Bauer, Chirality as generalized spin-orbit interaction in spintronics, *Phys. Rep.* **1009**, 1 (2023).
- [61] M. Kugler, G. Brandl, J. Waizner, M. Janoschek, R. Georgii, A. Bauer, K. Seemann, A. Rosch, C. Pfeleiderer, P. Böni, and M. Garst, Band structure of helimagnons in MnSi resolved by inelastic neutron scattering, *Phys. Rev. Lett.* **115**, 097203 (2015).
- [62] T. Schwarze, J. Waizner, M. Garst, A. Bauer, M. Janoschek, P. Pfeleiderer, C. Pfeleiderer, and D. Grundler, Universal helimagnon and skyrmion excitations in metallic, semiconducting and insulating chiral magnets, *Nat. Mater.* **14**, 478 EP (2015).
- [63] M. Weiler, A. Aqeel, M. Mostovoy, A. Leonov, S. Geprägs, R. Gross, H. Huebl, T. T. M. Palstra, and S. T. B. Goennenwein, Helimagnon resonances in an intrinsic chiral magnonic crystal, *Phys. Rev. Lett.* **119**, 237204 (2017).
- [64] M. Garst, J. Waizner, and D. Grundler, Collective spin excitations of helices and magnetic skyrmions: review and perspectives of magnonics in non-centrosymmetric magnets, *J. Phys. D: Appl. Phys.* **50**, 293002 (2017).
- [65] C. Ríos-Venegas, F. Brevis, R. A. Gallardo, and P. Landeros, Dynamic origin of conical helix magnetization textures stabilized by Dzyaloshinskii-Moriya interaction,

- Phys. Rev. B* **105**, 224403 (2022).
- [66] J. Rowland, S. Banerjee, and M. Randeria, Skyrmions in chiral magnets with Rashba and Dresselhaus spin-orbit coupling, *Phys. Rev. B* **93**, 020404 (2016).
- [67] B. Göbel, A. Mook, J. Henk, and I. Mertig, Magnetoelectric effect and orbital magnetization in skyrmion crystals: Detection and characterization of skyrmions, *Phys. Rev. B* **99**, 060406 (2019).
- [68] S. Bhowal and N. A. Spaldin, Magnetoelectric classification of skyrmions, *Phys. Rev. Lett.* **128**, 227204 (2022).
- [69] F. N. Rybakov, N. S. Kiselev, A. B. Borisov, L. Döring, C. Melcher, and S. Blügel, Magnetic hopfions in solids, *APL Mater.* **10**, 111113 (2022).
- [70] C. Saji, R. E. Troncoso, V. L. Carvalho-Santos, D. Altbir, and A. S. Nunez, Hopfion-driven magnonic Hall effect and magnonic focusing, *Phys. Rev. Lett.* **131**, 166702 (2023).
- [71] R. A. Pepper, M. Beg, D. Cortés-Ortuño, T. Kluyver, M.-A. Bisotti, R. Carey, M. Vousden, M. Albert, W. Wang, O. Hovorka, and H. Fangohr, Skyrmion states in thin confined polygonal nanostructures, *J. Appl. Phys.* **123**, 093903 (2018).
- [72] D. Cortés-Ortuño, N. Romming, M. Beg, K. von Bergmann, A. Kubetzka, O. Hovorka, H. Fangohr, and R. Wiesendanger, Nanoscale magnetic skyrmions and target states in confined geometries, *Phys. Rev. B* **99**, 214408 (2019).
- [73] N. Mehmood, R. Fazal, W. Yadong, T. Guo, Q. Zhang, Z. Hou, G. Xingsen, and J.-M. Liu, Stability phase diagrams and tuning of magnetic skyrmionium and other states, *J. Magn. Magn. Mater.* **526**, 167706 (2021).
- [74] M. Ponsudana, R. Amuda, R. Madhumathi, A. Brinda, and N. Kanimozhi, Confinement of stable skyrmionium and skyrmion state in ultrathin nanoring, *Physica B: Condens. Matter* **618**, 413144 (2021).
- [75] X. Xing, Y. Zhou, and H. Braun, Magnetic skyrmion tubes as nonplanar magnonic waveguides, *Phys. Rev. Appl.* **13**, 034051 (2020).
- [76] J. A. Otálora, M. Yan, H. Schultheiss, R. Hertel, and A. Kákay, Curvature-induced asymmetric spin-wave dispersion, *Phys. Rev. Lett.* **117**, 227203 (2016).
- [77] D. D. Sheka, O. V. Pylypovskiy, P. Landeros, Y. Gaididei, A. Kákay, and D. Makarov, Nonlocal chiral symmetry breaking in curvilinear magnetic shells, *Communications Physics* **3**, 128 (2020).
- [78] M. M. Salazar-Cardona, L. Körber, H. Schultheiss, K. Lenz, A. Thomas, K. Nielsch, A. Kákay, and J. A. Otálora, Nonreciprocity of spin waves in magnetic nanotubes with helical equilibrium magnetization, *Appl. Phys. Lett.* **118**, 262411 (2021).
- [79] R. Gallardo, P. Alvarado-Seguel, and P. Landeros, Unidirectional chiral magnonics in cylindrical synthetic antiferromagnets, *Phys. Rev. Appl.* **18**, 054044 (2022).
- [80] L. Körber, M. Zimmermann, S. Wintz, S. Finizio, M. Kronseder, D. Bougeard, F. Dirnberger, M. Weigand, J. Raabe, J. A. Otálora, H. Schultheiss, E. Josten, J. Lindner, I. Kézsmárki, C. H. Back, and A. Kákay, Symmetry and curvature effects on spin waves in vortex-state hexagonal nanotubes, *Phys. Rev. B* **104**, 184429 (2021).
- [81] K. V. Yershov, V. P. Kravchuk, D. D. Sheka, and U. K. Röbber, Curvature effects on phase transitions in chiral magnets, *SciPost Phys.* **9**, 043 (2020).
- [82] B. Mimiça-Figari, F. Brevis, D. Cortés-Ortuño, R. A. Gallardo, and P. Landeros, Magnetic textures in nanotubes with interfacial Dzyaloshinskii-Moriya interaction, unpublished (2024).
- [83] R. A. Gallardo, P. Alvarado-Seguel, F. Brevis, A. Roldán-Molina, K. Lenz, J. Lindner, and P. Landeros, Spin-wave channeling in magnetization-graded nanostrips, *Nanomaterials* **12**, 2785 (2022).
- [84] M. Mruczkiewicz, P. Graczyk, P. Lupo, A. Adeyeye, G. Gubbiotti, and M. Krawczyk, Spin-wave nonreciprocity and magnonic band structure in a thin permalloy film induced by dynamical coupling with an array of nit stripes, *Phys. Rev. B* **96**, 104411 (2017).
- [85] M. Grassi, M. Geilen, D. Louis, M. Mohseni, T. Brächer, M. Hehn, D. Stoeffler, M. Bailleul, P. Pirro, and Y. Henry, Slow-wave-based nanomagnonic diode, *Phys. Rev. Applied* **14**, 024047 (2020).
- [86] M. A. Kuznetsov and A. A. Fraerman, Temperature-sensitive spin-wave nonreciprocity induced by interlayer dipolar coupling in ferromagnet/paramagnet and ferromagnet/superconductor hybrid systems, *Phys. Rev. B* **105**, 214401 (2022).
- [87] In Ref. [86], the calculated frequency asymmetry Δf is proportional to $\mathbf{k} \cdot (\mathbf{n} \times \mathbf{M})$, which agrees with the nonreciprocity condition if $\boldsymbol{\tau} \rightarrow \mathbf{n} \times \mathbf{M}$.
- [88] L. Tan, G. Ma, S. Zheng, M. Liu, J. Min, J. Zhang, Y. Li, Y. Xie, Z. Ma, Y. Zhang, L. Lin, X. Wang, H. Li, S. Dong, and J.-M. Liu, Possible role of toroidal moments and Dzyaloshinskii-Moriya interaction in the magnetoelectric effect of the hyperkagome compound $\text{Mn}_3\text{Al}_2\text{Ge}_3\text{O}_{12}$, *Phys. Rev. B* **110**, 245116 (2024).
- [89] S. Hayami, Y. Yanagi, and H. Kusunose, Spontaneous antisymmetric spin splitting in noncollinear antiferromagnets without spin-orbit coupling, *Phys. Rev. B* **101**, 220403 (2020).
- [90] S. Hayami, Y. Yanagi, and H. Kusunose, Bottom-up design of spin-split and reshaped electronic band structures in antiferromagnets without spin-orbit coupling: Procedure on the basis of augmented multipoles, *Phys. Rev. B* **102**, 144441 (2020).

Supplementary material for *The Toroidal Moments in Confined Nanomagnets and its Impact on Magnonics*

F. Brevis,^{1,*} L. Körber,² R. A. Gallardo,¹ A. Kákay,³ and P. Landeros^{1,†}

¹*Departamento de Física, Universidad Técnica Federico Santa María, Avenida España 1680, Valparaíso, Chile*

²*Radboud University, Institute of Molecules and Materials,
Heyendaalseweg 135, 6525 AJ Nijmegen, The Netherlands*

³*Helmholtz-Zentrum Dresden-Rossendorf, Institute of Ion Beam Physics and Materials Research,
Bautzner Landstr. 400, 01328 Dresden, Germany*

(Dated: December 19, 2024)

This Supplementary Material provides a detailed account of the main calculations, starting with the derivation of the surface toroidal moment. Next, the expressions for the toroidal moment arising from well-known magnetic textures are computed.

I. ANALYTICAL DERIVATION OF THE SURFACE TOROIDAL MOMENT

The toroidal moment associated with any current proposed by Dubovik and Tugushev [1] is

$$\boldsymbol{\tau} = \frac{1}{10} \int dV [\mathbf{r}(\mathbf{r} \cdot \mathbf{J}) - 2r^2 \mathbf{J}]. \quad (1)$$

In order to investigate the connection between the magnetization (\mathbf{M}) and the toroidal moment ($\boldsymbol{\tau}$), consider that a magnetization distribution may create a bound current (\mathbf{J}_b), defined as

$$\mathbf{J}_b(\mathbf{r}) = \nabla \times \mathbf{M}, \quad (2)$$

and in the absence of free and polarization currents, $\mathbf{J} = \mathbf{J}_b$. Replacing this expression into the Eq (1),

$$\boldsymbol{\tau} = \frac{1}{10} \int dV [\mathbf{r}(\mathbf{r} \cdot (\nabla \times \mathbf{M})) - 2r^2(\nabla \times \mathbf{M})]. \quad (3)$$

As $\nabla \times \mathbf{r} = 0$, then, the divergence of a cross-product can be written as

$$\nabla \cdot (\mathbf{r} \times \mathbf{M}) = -\mathbf{r} \cdot (\nabla \times \mathbf{M}). \quad (4)$$

On the other hand, the curl of the product between a scalar function ψ and a vector function \mathbf{M} can be expanded as

$$\nabla \times (\psi \mathbf{M}) = \psi(\nabla \times \mathbf{M}) + (\nabla \psi) \times \mathbf{M}. \quad (5)$$

Considering that $\psi = -2r^2$, the second term in Eq. 3 gives

$$-2r^2(\nabla \times \mathbf{M}) = -2\nabla \times (r^2 \mathbf{M}) + 4\mathbf{r} \times \mathbf{M}, \quad (6)$$

then, the toroidal moment becomes

$$\boldsymbol{\tau} = \frac{1}{10} \int dV [-\mathbf{r}[\nabla \cdot (\mathbf{r} \times \mathbf{M})] - 2\nabla \times (r^2 \mathbf{M}) + 4\mathbf{r} \times \mathbf{M}]. \quad (7)$$

From vector calculus identities,

$$\int_V dV \psi \nabla \cdot \mathbf{A} = \oint_S \psi \mathbf{A} \cdot d\mathbf{S} - \int_V dV \mathbf{A} \cdot \nabla \psi. \quad (8)$$

* felipe.brevis@usm.cl

† pedro.landeros@usm.cl

On the other hand, in Cartesian coordinates, it can be considered that,

$$\int dV \mathbf{r}[\nabla \cdot (\mathbf{r} \times \mathbf{M})] = \hat{r}_i \int dV r_i[\nabla \cdot (\mathbf{r} \times \mathbf{M})] \quad (9)$$

Where $r_i = x, y, z$, and the Einstein notation is used. Considering $\psi = r_i$ and $\mathbf{A} = \mathbf{r} \times \mathbf{M}$, then

$$\int_V dV r_i \nabla \cdot (\mathbf{r} \times \mathbf{M}) = \oint_S r_i (\mathbf{r} \times \mathbf{M}) \cdot d\mathbf{S} - \int_V dV (\mathbf{r} \times \mathbf{M}) \cdot \nabla r_i, \quad (10)$$

but we have that $\nabla r_i = \hat{r}_i$, then

$$\int_V dV r_i \nabla \cdot (\mathbf{r} \times \mathbf{M}) = \oint_S r_i (\mathbf{r} \times \mathbf{M}) \cdot d\mathbf{S} - \int_V dV (\mathbf{r} \times \mathbf{M})_i, \quad (11)$$

and adding the three components,

$$\hat{r}_i \int_V dV r_i \nabla \cdot (\mathbf{r} \times \mathbf{M}) = \hat{r}_i \oint_S r_i (\mathbf{r} \times \mathbf{M}) \cdot d\mathbf{S} - \int_V dV (\mathbf{r} \times \mathbf{M}). \quad (12)$$

Replacing the obtained result into the toroidal moment in Eq. 7,

$$\boldsymbol{\tau} = -\frac{1}{10} \oint_S dS \mathbf{r}[(\mathbf{M} \times \mathbf{n}) \cdot \mathbf{r}] - \frac{2}{5} \int dV \nabla \times (r^2 \mathbf{M}) + \frac{1}{2} \int dV \mathbf{r} \times \mathbf{M}. \quad (13)$$

The volume integral of the curl of a function, which can be obtained from the Gauss Theorem, is

$$\int_V dV \nabla \times \mathcal{G} = - \oint_S \mathcal{G} \times d\mathbf{S}. \quad (14)$$

By considering that $\mathcal{G} = r^2 \mathbf{M}$ and $d\mathbf{S} = \mathbf{n} dS$ where \mathbf{n} is the unit vector normal to the surface,

$$\boldsymbol{\tau} = -\frac{1}{10} \oint_S dS \mathbf{r}[(\mathbf{M} \times \mathbf{n}) \cdot \mathbf{r}] + \frac{1}{5} \oint_S dS r^2 (\mathbf{M} \times \mathbf{n}) + \frac{1}{2} \int dV \mathbf{r} \times \mathbf{M}. \quad (15)$$

It follows that $\mathbf{M} \times \mathbf{n}$ corresponds to the bound surface current \mathbf{K}_b [2], and the toroidal moment is

$$\boldsymbol{\tau} = \frac{1}{2} \int_V dV (\mathbf{r} \times \mathbf{M}) - \frac{1}{10} \oint_S dS [\mathbf{r}(\mathbf{r} \cdot \mathbf{K}_b) - 2r^2 \mathbf{K}_b]. \quad (16)$$

Then, the toroidal moment splits into two contributions, $\boldsymbol{\tau} = \boldsymbol{\tau}^v + \boldsymbol{\tau}^s$, where

$$\boldsymbol{\tau}^v = \frac{1}{2} \int_V dV (\mathbf{r} \times \mathbf{M}) \quad (17)$$

is the volume term and the standard expression to evaluate the toroidal moment [3, 4], and

$$\boldsymbol{\tau}^s = -\frac{1}{10} \oint_S dS [\mathbf{r}(\mathbf{r} \cdot \mathbf{K}_b) - 2r^2 \mathbf{K}_b] \quad (18)$$

is the emergent toroidal moment due to surface-bound current \mathbf{K}_b . Notice that $\boldsymbol{\tau}^s$ is analogous to Eq. (1) but with a closed surface integral and opposite sign.

II. TOROIDAL MOMENTS OF THE STUDIED MAGNETIC TEXTURES

In this section, the volume and surface toroidal moments are calculated for various noncollinear magnetic states including the conical-helix textures in planar and tubular systems and skyrmionic magnetizations such as the skyrmion, bimeron and meron.

A. Analytical expressions for toroidal moments from conical-helix texture.

Using the model for the conical-helix texture magnetization described in the main text, the surface and volume toroidal moments, $\boldsymbol{\tau}^s$ and $\boldsymbol{\tau}^v$ respectively, calculated with respect to the geometric center of an ultrathin squared film with area L^2 and thickness d , are given by

$$\boldsymbol{\tau}^s = \sin \theta \begin{pmatrix} \mathcal{A}_1^s \sin \psi \cos \varphi_{\mathbf{q}} \\ -\mathcal{A}_1^s \sin \psi \sin \varphi_{\mathbf{q}} \\ \mathcal{A}_2^s \cos \psi \cos \varphi_{\mathbf{q}} \end{pmatrix} \quad (19)$$

and

$$\boldsymbol{\tau}^v = \mathcal{B}^v \sin \theta \begin{pmatrix} \sin \psi \cos \varphi_{\mathbf{q}} \\ -\sin \psi \sin \varphi_{\mathbf{q}} \\ \cos \psi \cos \varphi_{\mathbf{q}} \end{pmatrix}, \quad (20)$$

where \mathcal{A}_1^s , \mathcal{A}_2^s and \mathcal{B}^v are

$$\mathcal{A}_1^s = \frac{M_s d L}{60 q^2} \left[(2d^2 q^2 + 7L^2 q^2 + 12) \sin \left(\frac{Lq}{2} \right) - 6Lq \cos \left(\frac{Lq}{2} \right) \right], \quad (21)$$

$$\mathcal{A}_2^s = \frac{M_s d L}{60 q^2} \left[(d^2 q^2 + 8L^2 q^2 + 12) \sin \left(\frac{Lq}{2} \right) - 6Lq \cos \left(\frac{Lq}{2} \right) \right], \quad (22)$$

$$\mathcal{B}^v = \frac{M_s d L}{2 q^2} \left[Lq \cos \left(\frac{Lq}{2} \right) - 2 \sin \left(\frac{Lq}{2} \right) \right]. \quad (23)$$

An oscillatory behavior around $Lq/2$ is a prominent feature, which may result in positive, zero, or negative toroidal moments. In the ultrathin limit $L \gg d$, all the terms proportional to $(qd)^2$ are negligible. When comparing $\boldsymbol{\tau}^v$ with $\boldsymbol{\tau}^s$ it is interesting to note that despite their differences, the resulting toroidal moments are parallel to each other and always perpendicular to the respective pitch vector (\mathbf{q}) despite the choice of origin. Table I summarizes the toroidal moment directions for this texture and for both interfacial and bulk Dzyaloshinskii-Moriya interactions (b-DMI and i-DMI).

TABLE I. Summary of the surface toroidal moment directions for the conical helix with bulk and interfacial DMI and for the two relevant phase constants appropriate to in-plane ($\psi = \pi/2$) and out-of-plane ($\psi = 0$) magnetic films. The brackets show the pairs of surfaces contributing to $\boldsymbol{\tau}^s$.

Conical-helix	b-DMI	i-DMI
ψ	$(\varphi_{\mathbf{q}} = 0, \mathbf{q} = q \hat{y})$	$(\varphi_{\mathbf{q}} = \pi/2, \mathbf{q} = q \hat{x})$
$\pi/2$	$(\tau_x^s, 0, 0) \{S_x, S_y\}$	$(0, \tau_y^s, 0) \{S_x, S_y\}$
0	$(0, 0, \tau_z^s) \{S_y, S_z\}$	0

Fig. 1 shows the dependence of $\boldsymbol{\tau}^v$ with the lateral size L for fixed parameters and for both types of DMI. It can be seen that a difference between b-DMI ($\varphi_{\mathbf{q}} = 0$) and i-DMI ($\varphi_{\mathbf{q}} = \pi/2$) is the sign and the direction of $\boldsymbol{\tau}$ when $\psi = \pi/2$. For the other case, $\psi = 0$, a nonzero $\boldsymbol{\tau}$ is seen only for b-DMI, while for i-DMI, it cancels out. By analyzing the surface contribution, it is observed that for b-DMI, there is a slight difference in the amplitudes when comparing $\psi = 0$ and $\psi = \pi/2$, which is not the case for $\boldsymbol{\tau}^v$. In spite there is only one case in which $\boldsymbol{\tau}$ is always zero (for i-DMI and $\psi = 0$), for all other configurations of $\varphi_{\mathbf{q}}$ and ψ , the toroidal moment could be zero for specific values of $Lq/2$, which is due to commensurability. For the configurations studied, it is observed that $\boldsymbol{\tau}^v$ and $\boldsymbol{\tau}^s$ are always parallel to either x , y , or z depending on the type of DMI ($\varphi_{\mathbf{q}}$) and phase (ψ).

In order to describe the surface toroidal moment ($\boldsymbol{\tau}^s$) it is necessary to identify which faces contribute to its formation. Given the cuboid geometry of the sample, the surfaces are grouped by the direction of its normal vector, where S_x , S_y , and S_z refers to each pair of surfaces. Table I indicates the faces contributing to $\boldsymbol{\tau}^s$ in curly brackets. It is found, surprisingly, that for low perpendicular anisotropy ($\psi = \pi/2$), the surfaces contributing to $\boldsymbol{\tau}^s$ are the lateral edges (S_x, S_y) with area Ld . In contrast, for the surviving $\boldsymbol{\tau}$ when $\psi = 0$, the contributing pair of surfaces are S_y and S_z , where S_z have an area L^2 much larger than for $S_{x,y}$. From the point of view of the amplitudes, no significant difference is predicted when comparing $\psi = 0$ and $\psi = \pi/2$ for b-DMI as mentioned above; it is inferred then that the size of the areas is not particularly relevant, but rather the direction of their normal vectors.

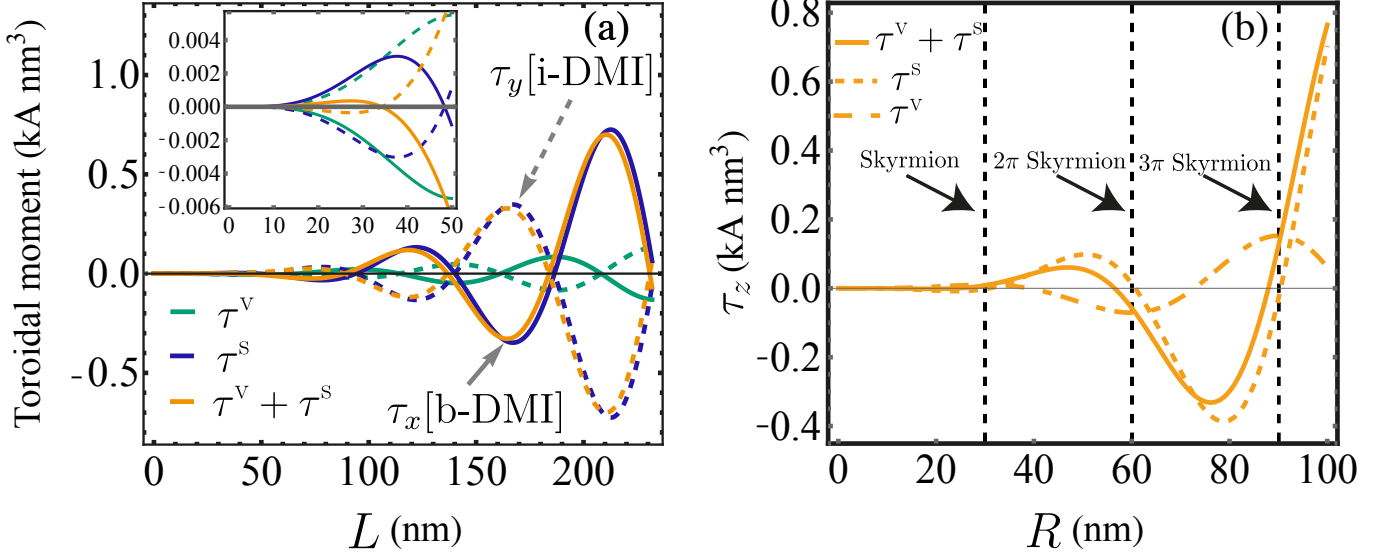


FIG. 1. (a) Nonzero components of the toroidal moments τ^v , τ^s , and their sum τ , for the conical-helix texture as a function of the film size L . The DMI strength is fixed at $D = 3 \text{ mJ/m}^2$, and the magnetic phase ($\psi = \pi/2$) correspond to a film with low perpendicular anisotropy. Continuous (segmented) curves correspond to bulk (interfacial) DMI with $x(y)$ -component, and the inset corresponds to a zoom of the first tens of nanometers. (b) Toroidal moments (z -component) for Bloch skyrmion-like states ($\gamma = \pi/2$) as a function of the nanodot radius when $\lambda = 30 \text{ nm}$.

B. Analytical expressions for toroidal moments from Skyrmion, bimeron and meron.

The chosen model for the skyrmionic textures is given by $\mathbf{M} = M_s [\sin \theta(\mathbf{r}) \cos(\phi + \gamma) \hat{x} + \sin \theta(\mathbf{r}) \sin(\phi + \gamma) \hat{y} + \cos \theta(\mathbf{r}) \hat{z}]$ [4], where $\theta(\mathbf{r}) = \pi(1 - r/\lambda)$, with λ a characteristic radius for which $\mathbf{M}(r = \lambda) = -\mathbf{M}(0)$, $0 \leq \phi \leq 2\pi$ and γ is the helicity: $\gamma = 0(\pi/2)$ corresponds to a Néel (Bloch) skyrmion. The same expression can describe the antiskyrmion, by making $\phi \rightarrow -\phi$, while the bimeron texture is obtained by considering a y -axis rotation in 90° , which implies $M_x \rightarrow M_z$, $M_y \rightarrow M_y$ and $M_z \rightarrow -M_x$. From this, it is possible to model Skyrmioniums or $\ell\pi$ -Skyrmions ($\ell = 1, 2, 3, \dots$) and $R = \ell\lambda$, which are skyrmion-like states stabilized in a ferromagnetic nanodisk of radius R and thickness d . They are composed of a combination of skyrmions or multiple full spin rotations along the diameter with a different topological charge [5–8]. We also considered a linear meron model [9], given by $\mathbf{M} = M_s [-\sin \theta(r) \sin \phi \hat{x} + \sin \theta(r) \cos \phi \hat{y} + \cos \theta(r) \hat{z}]$, where $\theta = \frac{\pi r}{2R}$ for $r \leq R$. Table II summarizes the volumetric and surface toroidal moments with their contributing faces and the Fig. 2 shows the dependence of the relevant components of τ^v with the helicity (γ). It can be seen from the Table II and the Fig. 2 that for $\gamma = 0$, τ^v is always zero, then Néel-like textures do not induce dipolar nonreciprocity. Note that full skyrmioniums are composed of integer values of ℓ ; however, a non-integer value was chosen in Fig. 2 for instructive reasons, since for integer values τ^s is always zero for bimerons.

TABLE II. Surface and volume toroidal moments for Skyrmion, bimeron, and meron. For antiskyrmion both toroidal moments are always zero. The brackets show the pairs of surfaces contributing to τ^s .

	Skyrmion	Bimeron	Meron
τ^s	$C^s(0, 0, \sin \gamma) \{S_z\}$	$(D_1^s \sin \gamma, D_1^s \cos \gamma, D_2^s \sin \gamma) \{S_z\}$	$(0, 0, \mathcal{E}^s) \{S_z, S_\rho\}$
τ^v	$C^v(0, 0, \sin \gamma)$	$D^v(\sin \gamma, \cos \gamma, \sin \gamma)$	$(0, 0, \mathcal{E}^v)$

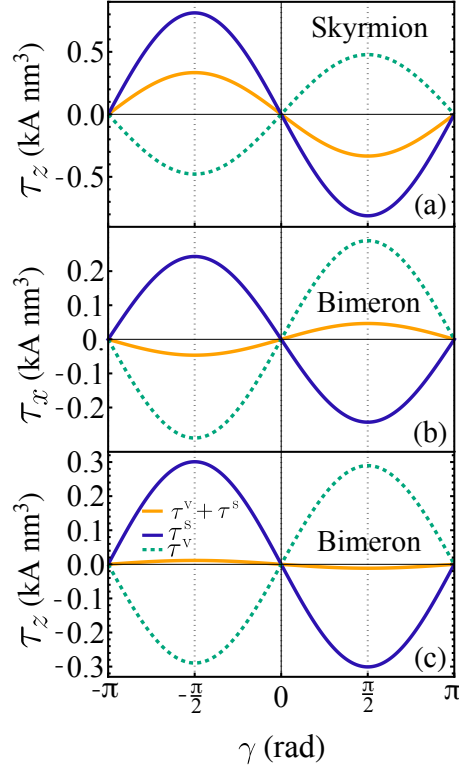


FIG. 2. Relevant components of the volume toroidal moment as a function of the magnetic helicity γ for different textures: (a) skyrmion (z -component) and (b,c) bimeron (x - and z -components) for $R = 100$ nm, $d = 1$ nm, $M_s = 658$ kA/m and $\lambda = 5R/4$.

The corresponding expressions that appears in Table II are

$$\mathcal{C}^s = -M_s d \frac{\pi R [\pi^2 d^2 + 24(\lambda^2 + \pi^2 R^2)] \sin\left(\frac{\pi R}{\lambda}\right) - 24\lambda^3 + 12\lambda(2\lambda^2 - \pi^2 R^2) \cos\left(\frac{\pi R}{\lambda}\right)}{60\pi^2}, \quad (24)$$

$$\mathcal{C}^v = M_s d \lambda \frac{(2\lambda^2 - \pi^2 R^2) \cos\left(\frac{\pi R}{\lambda}\right) - 2\lambda[\lambda - \pi R \sin\left(\frac{\pi R}{\lambda}\right)]}{\pi^2}, \quad (25)$$

$$\mathcal{D}_1^s = -M_s \pi R d (d^2 + 12R^2) \sin\left(\frac{\pi R}{\lambda}\right), \quad (26)$$

$$\mathcal{D}_2^s = -M_s d \frac{\pi R [\pi^2 d^2 + 24(\lambda^2 + \pi^2 R^2)] \sin\left(\frac{\pi R}{\lambda}\right) - 24\lambda^3 + 12\lambda(2\lambda^2 - \pi^2 R^2) \cos\left(\frac{\pi R}{\lambda}\right)}{120\pi^2}, \quad (27)$$

$$\mathcal{D}^v = M_s d \lambda \frac{(2\lambda^2 - \pi^2 R^2) \cos\left(\frac{\pi R}{\lambda}\right) - 2\lambda[\lambda - \pi R \sin\left(\frac{\pi R}{\lambda}\right)]}{2\pi^2}, \quad (28)$$

$$\mathcal{E}^s = -M_s d R \frac{\pi^3 d^2 + 24R^2(\pi^3 + 4\pi - 8)}{60\pi^2}, \quad (29)$$

$$\mathcal{E}^v = M_s d R^3 \frac{8(\pi - 2)}{\pi^2} \quad (30)$$

C. Toroidal moment of conical-helix texture on thin tubes

By considering the following model for a conical-helix magnetization distributed over a thin tubular shell [10],

$$\frac{\mathbf{M}}{M_s} = \cos(n\phi + q_z z + \psi) \sin\theta \hat{\rho} + \sin(n\phi + q_z z + \psi) \sin\theta \hat{\phi} + \cos\theta \hat{z} \quad (31)$$

where n is the azimuthal index which quantizes the azimuthal component of the pitch vector, q_z is the z -component of the pitch vector, ψ is a phase and θ is the cone angle.

the volume toroidal moment from Eq. 17 gives

$$\boldsymbol{\tau}^v = \frac{1}{2} \int dV \{-z \sin \theta \sin(q_z z + n\phi + \psi) \hat{\rho} + [z \sin \theta \cos(q_z z + n\phi + \psi) - \rho \cos \theta] \hat{\phi} + \rho \sin \theta \sin(q_z z + n\phi + \psi) \hat{z}\}. \quad (32)$$

By changing from cylindrical to Cartesian unitary vectors, i.e., $(\hat{\rho}, \hat{\phi}, \hat{z}) \rightarrow (\hat{x}, \hat{y}, \hat{z})$, and integrating in cylindrical coordinates for a thin tube with inner radius βR , outer radius R and length L , $\boldsymbol{\tau}^v$ becomes

$$\begin{aligned} \boldsymbol{\tau}^v = M_s R^2 \sin \theta \sin(n\pi) & \left\{ \frac{(1 - \beta^2) \cos(n\pi + \psi)}{2q_z^2(n+1)} \left[q_z L \cos\left(\frac{q_z L}{2}\right) - 2 \sin\left(\frac{q_z L}{2}\right) \right] \hat{x} \right. \\ & + \frac{(1 - \beta^2) \sin(n\pi + \psi)}{2q_z^2(n+1)} \left[q_z L \cos\left(\frac{q_z L}{2}\right) - 2 \sin\left(\frac{q_z L}{2}\right) \right] \hat{y} \\ & \left. + \frac{2(1 - \beta^3) R}{3q_z n} \sin\left(\frac{q_z L}{2}\right) \sin(n\pi + \psi) \hat{z} \right\}. \end{aligned} \quad (33)$$

By inspecting the q_z and n values it is found that this expression is only nonzero for $n = 0$ and $n = -1$ and the result can be expressed as

$$\begin{aligned} \boldsymbol{\tau}^v = M_s \frac{2\pi(1 - \beta^3) R^3}{3q_z} \sin \theta \sin \psi \sin\left(\frac{q_z L}{2}\right) \delta_{n,0} \hat{z} \\ + M_s \frac{\pi R^2(1 - \beta^2)}{2q_z^2} \sin \theta \left[q_z L \cos\left(\frac{q_z L}{2}\right) - 2 \sin\left(\frac{q_z L}{2}\right) \right] \delta_{n,-1} (\cos \psi \hat{x} + \sin \psi \hat{y}). \end{aligned} \quad (34)$$

where the symbol $\delta_{i,j}$ denotes the Kronecker delta function. For the particular case $q_z = 0$ and $n = 0$,

$$\boldsymbol{\tau}^v = M_s \frac{LR^3}{3} \pi (1 - \beta^3) \sin \theta \sin \psi \hat{z}. \quad (35)$$

On the other hand, the toroidal moment $\boldsymbol{\tau}$ (Eq. 1) for the same texture is given by,

$$\begin{aligned} \boldsymbol{\tau} = \frac{M_s \pi (\beta - 1) R \sin \theta \sin \psi}{30q_z^3} & \left[\sin\left(\frac{q_z L}{2}\right) (q_z^2 (3L^2 + 4(\beta^2 + \beta + 1)R^2) - 24) \right. \\ & \left. + 2q_z L \cos\left(\frac{q_z L}{2}\right) ((\beta^2 + \beta + 1)q_z^2 R^2 + 6) \right] \hat{z} \delta_{n,0} \\ - \frac{M_s \pi (\beta^2 - 1) R^2 \sin \theta}{20q_z^2} & \left[\sin\left(\frac{q_z L}{2}\right) (q_z^2 (2L^2 + 3(\beta^2 + 1)R^2) - 16) + 8q_z L \cos\left(\frac{q_z L}{2}\right) \right] (\cos \psi \hat{x} + \sin \psi \hat{y}) \delta_{n,-1} \\ + \frac{M_s \pi (\beta^2 - 1) R^2 \sin \theta}{20q_z^2} & \left[\sin\left(\frac{q_z L}{2}\right) ((\beta^2 + 1)q_z^2 R^2 - 4) + 2q_z L \cos\left(\frac{q_z L}{2}\right) \right] (\cos \psi \hat{x} - \sin \psi \hat{y}) \delta_{n,1}. \end{aligned} \quad (36)$$

This last expression is only nonzero for $n = -1$, $n = 0$ and $n = 1$. Analogously, the surface toroidal moment $\boldsymbol{\tau}^s$ for this texture using the Eq. 18 is

$$\begin{aligned} \boldsymbol{\tau}^s = \frac{M_s \pi (\beta - 1) R \sin \theta \sin \psi}{30q_z^3} & \left[3 \sin\left(\frac{q_z L}{2}\right) (q_z^2 (L^2 + 8(\beta^2 + \beta + 1)R^2) - 8) \right. \\ & \left. + 2q_z L \cos\left(\frac{q_z L}{2}\right) ((\beta^2 + \beta + 1)q_z^2 R^2 + 6) \right] \hat{z} \delta_{n,0} \\ - \frac{M_s \pi (\beta^2 - 1) R^2 \sin \theta \cos \psi}{20q_z^2} & \left[\sin\left(\frac{q_z L}{2}\right) (q_z^2 (2L^2 + 3(\beta^2 + 1)R^2) + 4) - 2q_z L \cos\left(\frac{q_z L}{2}\right) \right] \\ & \times (\cos \psi \hat{x} + \sin \psi \hat{y}) \delta_{n,-1} \\ + \frac{M_s \pi (\beta^2 - 1) R^2 \sin \theta}{20q_z^2} & \left[\sin\left(\frac{q_z L}{2}\right) ((\beta^2 + 1)q_z^2 R^2 - 4) + 2q_z L \cos\left(\frac{q_z L}{2}\right) \right] (\cos \psi \hat{x} - \sin \psi \hat{y}) \delta_{n,1}. \end{aligned} \quad (37)$$

which, as (36), is only non-zero for $n = 0$, $n = -1$ and $n = 1$. It can be noticed that the terms associated with $n = 1$ are exactly the same for $\boldsymbol{\tau}$ and $\boldsymbol{\tau}^s$ and because of that, those terms do not appear for $\boldsymbol{\tau}^v$.

- [2] D. J. Griffiths, *Introduction to electrodynamics* (Pearson, 2013).
- [3] N. A. Spaldin, M. Fiebig, and M. Mostovoy, The toroidal moment in condensed-matter physics and its relation to the magnetoelectric effect, *J. Phys. Condens. Matter.* **20**, 434203 (2008).
- [4] S. Bhowal and N. A. Spaldin, Magnetoelectric classification of skyrmions, *Phys. Rev. Lett.* **128**, 227204 (2022).
- [5] R. A. Pepper, M. Beg, D. Cortés-Ortuño, T. Kluyver, M.-A. Bisotti, R. Carey, M. Vousden, M. Albert, W. Wang, O. Hovorka, and H. Fangohr, Skyrmion states in thin confined polygonal nanostructures, *Journal of Applied Physics* **123**, 093903 (2018).
- [6] D. Cortés-Ortuño, N. Romming, M. Beg, K. von Bergmann, A. Kubetzka, O. Hovorka, H. Fangohr, and R. Wiesendanger, Nanoscale magnetic skyrmions and target states in confined geometries, *Phys. Rev. B* **99**, 214408 (2019).
- [7] N. Mehmood, R. Fazal, W. Yadong, T. Guo, Q. Zhang, Z. Hou, G. Xingsen, and J.-M. Liu, Stability phase diagrams and tuning of magnetic skyrmionium and other states, *Journal of Magnetism and Magnetic Materials* **526**, 167706 (2021).
- [8] M. Ponsudana, R. Amuda, R. Madhumathi, A. Brinda, and N. Kanimozhi, Confinement of stable skyrmionium and skyrmion state in ultrathin nanoring, *Physica B: Condensed Matter* **618**, 413144 (2021).
- [9] P. G. Radaelli, J. Radaelli, N. Waterfield-Price, and R. D. Johnson, Micromagnetic modeling and imaging of vortex|meron structures in an oxide|metal heterostructure, *Phys. Rev. B* **101**, 144420 (2020).
- [10] B. Mimiça-Figari, F. Brevis, D. Cortés-Ortuño, R. A. Gallardo, and P. Landeros, Magnetic textures in nanotubes with interfacial Dzyaloshinskii-Moriya interaction, unpublished (2024).